2023-05-01

Microscopic and Spectroscopic Analysis of Nordihydroguaiaretic Acid Effect on Astrocytes

Lizbeth Vanessa Martinez Lopez
University of Texas at El Paso

MICROSCOPIC AND SPECTROSCOPIC ANALYSIS OF NORDIHYDROGUAIARETIC ACID EFFECT ON ASTROCYTES

LIZBETH VANESSA MARTINEZ LOPEZ

Master's Program in Physics

APPROVED:

Felicia S. Manciu, Ph.D., Chair

Mark R. Pederson, Ph.D.

Emil Schwab, Ph.D.

Stephen L. Crites, Jr., Ph.D.
Dean of the Graduate School

Dedication

This thesis is dedicated to my beloved family. Their never-ending love and support with our combined efforts are why I can be exactly where I am today. Thank you for always believing in me.

MICROSCOPIC AND SPECTROSCOPIC ANALYSIS OF NORDIHYDROGUAIARETIC ACID EFFECT ON ASTROCYTES

by

LIZBETH VANESSA MARTINEZ LOPEZ, B.S.

THESIS

Presented to the Faculty of the Graduate School of

The University of Texas at El Paso

in Partial Fulfillment

of the Requirements

for the Degree of

MASTER OF SCIENCE

Department of Physics

THE UNIVERSITY OF TEXAS AT EL PASO

May 2023

Acknowledgements

I would like to express my deepest gratitude to my advisor, Dr. Felicia Manciu. Without her invaluable guidance and support, this work would have not been possible. Dr. Manciu provided me the opportunity to be part of her research group, where I acquired research and academic experience. This opportunity also helped me to grow not only as a scientist but as a person. Her feedback and every piece of advice given is deeply appreciated and will never be forgotten. I can say with certainty that I could not have asked for a better mentor.

I would like to thank Dr. Mark Pederson for his help and support, not only as my thesis committee but also as my professor and as the chair of the department. Dr. Pederson was always available to assist me with any complications that I encountered. His willingness to help and advise students, and his efforts to make the Department of Physics a comfortable environment, are deeply appreciated.

In addition, I am extremely grateful to Dr. Emil Schwab, who has taken the time out of his schedule to be a valuable member of my thesis committee. His assistance and provided knowledge and feedback, have been the very appreciated aid I needed to develop this work.

I had the pleasure to work with my group members in the Optical Spectroscopy and Microscopy lab, for all their help I would like to express my gratitude.

Finally, I would like to mention my family and friends, who always believed in me and gave me the courage and confidence to continue working on what I love. All of them have been the support I needed to complete this step toward my professional career.

Table of Contents

List of Tables

List of Figures

Chapter 1: Introduction

1.1 Introductory Remarks

The nervous system is divided into the peripheral nervous system (PNS) and the central nervous system (CNS). As every component of the body, it has its type of cells, specifically, neural cells. The neural cells in the nervous system are further divided into two main groups: neurons and glia. The glia cells, also known as neuroglia, can be found in both the PNS and CNS and are considered as non-excitable cells, contrary to the neurons. Our focus in this study is on specific type of cells that are called astrocytes, which are part of the central nervous system as well [1,2].

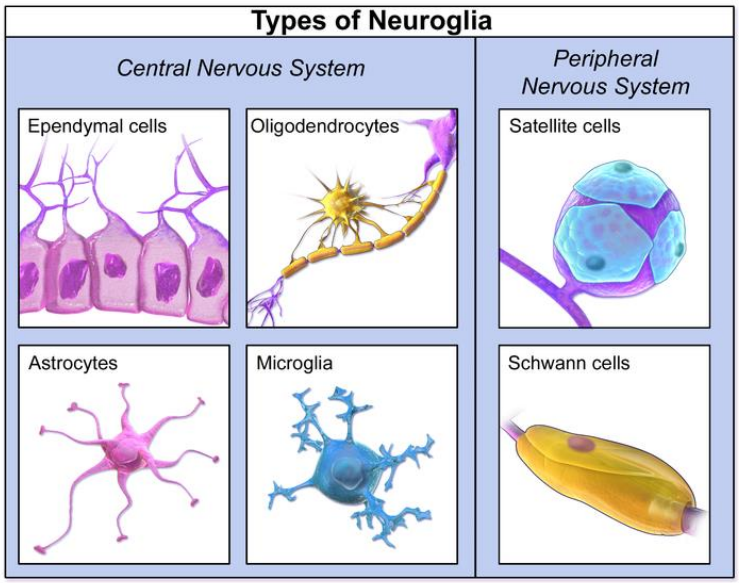

Figure 1.1. Types of glia/neuroglia cells. [3]

In the CNS we can find two types of glia cells, the macroglia and microglia. The astrocytes are part of the macroglia type along with the neural/glial antigen 2 (NG2-glia), and the oligodendrocytes [4]. As the name suggests, the astrocytes are cells with star-like shape [1].

Astrocytes are one of the most abundant cellular constituents of the CNS, since they represent between 20% and 50% of the total number of cells, depending on the living species [4, 5]. In the mammalian CNS, the percentage of astrocytes is around 40% from the total number of cells present in the brain [4, 6]. Besides being a major component of the CNS, astrocytes are also the most diverse type of cells [7].

1.2 Types of Astrocytes and Their Significance

The astrocytes are categorized based on their functional and morphological properties, hence their diversity. However, there are two main subtypes, the protoplasmic and fibrous astrocytes, represent the largest division and is based on their morphological properties. The protoplasmic astrocytes that are found in the gray matter and are widely branched and short. These characteristics allow them to develop into a further complicated ramification and to influence various bioprocesses. The fibrous astrocytes found in the white matter are less ramified. Besides their shapes suggesting their names, fibrous astrocytes are involved mainly in fiber-like processes [1,8].

Several and important functions of the astrocytes have been found by classical and modern studies of the nervous system anatomy. For instance, astrocytes execute primary homeostatic functions. These cells are an essential component of the blood–brain barrier (BBB). They perceive and react to outer insults-like bioprocess such as inflammation or injury, as well as take up metabolites to power the brain. Astrocytes and neurons have a dynamic and reciprocal interaction. The astrocytes collect glucose from the blood, circulating through the body, and either save it as glycogen or transform it to lactate to nourish active neurons. By giving trophic and metabolic assistance to neurons, astrocytes contribute to create a favorable condition in the brain. They

contribute to regulating —to mention a couple of processes— the neuronal activities and synapse formation and transmission. Astrocytes also have the capacity to take and metabolize neurotransmitters emitted through the synaptic pathway [4, 5,7,8].

Nonetheless, neurons are not the only components that have multiple bidirectional interactions with astrocytes. Another example are the blood vessels. The contact between blood vessels and astrocytes helps regulate the blood flow in the CNS by producing and releasing molecular mediators, which can change the diameter of the blood vessels and, consequently, increase or decrease the blood flow [8].

Furthermore, astrocytes play a variety of crucial roles in the formation of the gray and white matter. One of such roles is controlling the travel of emerging axons and of some neuroblasts, by forming molecular frontiers. In this context, it is worth mentioning that during the formation of the white matter a damage of the myelin layer can be caused by the loss or malfunction of astrocytes' connexins and gap junctions [8].

1.3 Contribution of Astrocytes to Brain Diseases

As mentioned before, astrocytes have an important role in homeostasis and neuronal development. Therefore, astrocyte malfunction can cause several neurodegenerative diseases (ND). We can find Alexander's disease as a clear example. Alexander's disease is a genetic, but rare, disorder where astrocyte's dysfunction is the main culprit. This disorder affects children and adults, and can lead to death. Alzheimer's disease, whose main targets are the elderly, is known to be the primary cause of dementia in this population. It is another example of neurological diseases where astrocytes are believed to have an important contribution and be one of the main causes [6]. Tumors and cancers are other examples, which are also the focus of the research

presented in this work. Such deceptive illnesses are caused by the uncontrollable proliferation of abnormal cells in one or various body areas [9].

Cells have their own life cycle — they grow, divide, and die. When this cycle changes and fails, the cells can form solid and non-solid tumors. When the tumor does not spread from the body area it was formed, it is called a benign tumor. On the contrary, when the tumor spreads to other areas and keeps growing, it is called a malignant tumor or a cancerous tumor. Usually, benign tumors are not considered dangerous nor life-threatening. However, if the tumor is found in the brain it can be lethal. Furthermore, tumors located in an area where they originally arose are called primary tumors. Tumors that spread to other body parts form the metastatic cancer [9].

1.4 Gliomas

Cancers and tumors are commonly named after the parts they arose. For instance, the CNS cancer consists of tumors and/or cancers originally created in the central nervous system. Gliomas are considered as one of the most common and aggressive tumors found in the CNS. As the name suggests, gliomas are tumors whose origin comes from the different glial cells. As previously mentioned, astrocytes are cells belonging to this category. As many other cells in the human body, there could be malignant tumors/types of cancer associated with them. Specifically for astrocytes, the astrocytoma and glioblastoma are most known [9,10].

The World Health Organization (WHO) classified gliomas according to their abnormality and severity. There are Grade I gliomas, which are often benign tumors, with an appearance similar to that of normal cells and that are slow growing. An example is the pilocytic astrocytomas. The Grade II gliomas, also known as diffuse gliomas, are slow-growing tumors that with time can develop into a more aggressive type; astrocytomas belong to this category. As a next stage we have

the Grade III gliomas, which are tumors poorly differentiated. In this category we can find one of the most malignant tumors derived from astrocytes called anaplastic astrocytomas. Finally, is the fast-growing and fast-spreading, highly malignant Grade IV gliomas, known as glioblastomas. This kind of tumors are undifferentiated, since they look different from the normal cells and tissue originating them [9,10].

Astrocytomas rarely spread to other body areas; they stay on the brain. However, since a lower-grade tumor can develop into one of these malignant gliomas, we can find secondary glioblastomas. In general, due to the growth of astrocytomas that reduce the space in the skull, the intracranial pressure increases. While the tumor does not metastasize to other body parts, it can cause damage in the normal brain function [10,11].

Anaplastic astrocytomas and glioblastomas are the most common malignant gliomas. They constitute 20% and 70% of the CNS tumors, respectively. Grade I glioma constitutes only 2% and Grade II about 8%. The first two lower grade gliomas are more common in children, while the Grade III and IV tumors are prevalent in adults. It has been reported an average survival rate of two years or less for glioblastomas and approximatively five years for anaplastic astrocytoma [9,10,11]. Furthermore, studies indicate that regardless of ethnicity, age, and other social factors, gliomas are predominantly encountered among men than women [9,10,11].

1.5 Potential Treatments of Gliomas

Nowadays, diagnosis for tumors start with methods based on reviews of patient medical history that looks for potential risk factors. It also includes a physical examination and more advanced, specific methods like Magnetic Resonance Imaging (MRI) and Computerized Tomography (CT) to help obtain the tumor's location and dimension, and Positron Emission

Tomography (PET) to look and analyze the affected area. Performing biopsies help with in vitro examining the tumor, by looking in detail for cancerous cells in the tissue removed from the body. Laboratory tests to look for alterations in some substance levels are other types of diagnosis methods for cancer and tumors. However, there is no current treatment given to patients with astrocytomas that can eliminate it completely. Surgery to remove a tumor, followed by radiotherapy to destroy cancer cells and/or chemotherapy to restrain cancer cells growing are usually the targeted therapy for these deadly brain diseases. In the case of lower grade gliomas, surgery is the only method to treat the tumor. For a high-grade astrocytoma, the common treatments are surgical resection, chemotherapy, or radiotherapy. It can also be a combination of them, since either chemo or radiotherapy follows usually a surgical resection [9].

Is important to emphasize that even with the existence of these different treatments, the outcome in patients with highly malignant brain tumors remains a devastating one. As we mentioned previously, the average survival rate for patients with anaplastic astrocytoma is around 2 to 5 years, while for glioblastomas is approximately 15 months. Extensive surgical resection of other organ's tumors such as breast and lung cancer, prolongs the survival rate of patients with this type of disease. However, a surgical approach of this nature is difficult in malignant astrocytomas because they spread and invade essential areas of the brain. Therefore, it remains unknown if an extensive surgical resection can prolong survival rate in astrocytoma patients [12].

Concerning general surgical resection, there are also other factors that can be associated with survival prolongation in pre-operative patients. These factors are age and functional status. It has been observed that the older the patient, the less chance of survival. This is because age increases the patient difficulty to resist neurological insults from the tumor itself and the surgery. The second factor leads to a similar observation; the poorer a patient's functional status is the more

decrease in its survival time. Since malignant gliomas are predominant in adults, we can assume that these factors may be the causes of these badly outcomes for these patients [12].

1.6 Alternative Approaches for Glioma Detection

The poor prognosis and patient survival rate in malignant astrocytomas have led scientists to search for better diagnosis and treatment alternatives. Even though neurosurgical approaches and resections are commonly used as main sources in determining the prognosis and the treatment, the difficulty to discriminate between the tumor and normal cells combined with the fact that the normal tissue must be preserved create additional differences and an increased variability. Furthermore, it is likely that remnant invasive tumor cells cannot be removed during the brain surgery completely. The infiltrative nature of astrocytoma makes it difficult for neurosurgeons to find the resection border, which is hardly distinguishable. The development of different techniques, such as intraoperative magnetic resonance imaging (MRI) to perform a safe and accurate tumor resection has been beneficial, but not sufficient. Therefore, it is a continuous need in modern medicine to develop new, fast, and precise methods that can help in discriminating tumors from healthy cells [13,14,15,16].

In recent years, Raman spectroscopy techniques have been employed as a useful tool to study brain cancer and healthy cells. This is in response to the need of an alternative, preoperative and/or intraoperative method that enables a full identification of tumor cell types. It has been established that Raman spectroscopy as an intraoperative technique has a sensitivity of 93% with a specificity of 91%. These specifications are good indicators for scientist prior to further develop and perfect this alternative approach for brain tumor analysis. It emphasizes that Raman-based techniques can be used to complement and/or replace common pathology laboratories techniques.

For instance, Raman scattering microscopy could be a good alternative for histopathology in biomedical imaging. However, due to some of the limitations that Raman spectroscopy and microscopy still have, it is necessary to conduct further and broader research, in-vitro and in-vivo, to overcome additional limitations for its clinical practicality [13].

Researchers have performed several experiments to test the functionality and benefit of different Raman spectroscopy techniques. An example is the research reported in 2007 by Banerjee and Zhang, who combined the use of optical tweezers and Raman spectroscopy to analyze brain cancer cells (astrocytoma) and normal astrocytes [16]. They found that the spectra of both type of cells although similar have a subtle difference regarding their intensities. A higher intensity in the spectra of cancer cells was an indication that there is a structural change in these cells that alter their functions was taking place. The results in this paper lead to the conclusion that Raman can be used for cancer diagnosis [16]. In 2014, Tanahashi, K. et. al. applied confocal Raman microscopy and statistical analysis in glioma cells and normal astrocytes. Similar to the Banerjee and Zhang results, they found that the signal for glioma cells were higher compared to that from the normal astrocytes. The discovers in this research proved once again that Raman spectroscopy is advantageous over the conventional diagnosis methods [15].

In a more recent research, Kowalska, A. A., et. al. (2020) proposed the combination between surface-enhanced Raman spectroscopy (SERS) and principal component analysis (PCA) as a practical alternative to conventional methods, due to a higher sensitivity and specificity. Several samples from the different lobes of the brain — anaplastic astrocytoma and glioblastoma— were collected for measurements. Several control samples were also considered for a better statistical precision. The SERS results reported in this article show that there are shifts in some of the bands belonging to certain components in the tumor tissues, such as nucleic acids or some

amino acids. For normal cells, it was found that the results/spectra exhibit a slight difference according to their locations. For instance, they observed that some band intensities are higher for the temporal cells located in the right brain hemisphere than those from the left brain hemisphere. They concluded that the observed changes in the spectra are due to the influence of the tumor in the normal brain cells. However, even though an analysis using only SERS spectra and images was possible, they stated that it will not be sufficient to make a diagnosis or provide an accurate differentiation between normal and tumor cells. To accomplish this, a combination of SERS with PCA is crucial [13].

Finding non-invasive methods for cancer treatments and diagnosis is still a challenge that scientists have. Extensive research is currently being done to contribute to the modern medicine advances regarding cancer. Not only does the previously mentioned examples support these statements, but also the purpose and direction of the current research project. Similar to, and advancing what have been done in research, our main focus is to employ the confocal Raman microscopy technique to analyze normal astrocyte and glioblastoma cells.

1.7 Alternative Approaches of Glioma Treatment

Majority of non-clinical studies were investigating the response of brain cancer to currently FDA approved drugs. Discovery and validation of new potential drugs is a continuous effort in the research community. To this end, the current work is intended to seek the potential of new chemical extract to prevent and alleviate brain cancer.

Larrea tridentata, also known as creosote bush, is a plant found in the deserts of the southwest of the United States and Mexico. The nordihydroguaiaretic acid (NDGA) is a phenolic lignan or plant metabolite, that is commonly extracted from the creosote bush. This plant has been

widely used in traditional medicine, mainly as an infusion from its leaves, to treat several diseases including cancer. It has been proved that NDGA is the main component that brings the beneficial results for different disorders, due its anti-inflammatory, antioxidant, and therapeutic effects [17,18]. Just as it has advantages, some studies have found that a constant intake of this infusion without any precaution can cause severe side effects [17,18]. For instance, kidney and liver damage had been reported. Being certain about the therapeutic effects of this lignan, which should not be ignored, scientists are still working in finding NDGA and its analogs potential for more target-selective drug administration, with a lower risk of toxicity. There is still more work and research to be done regarding this component, so it can be further understood concerning its safe pharmacological profile and in vivo applications [17].

In our previous study, we found that NDGA has therapeutic effects for glioblastoma multiforme. In this project, we analyzed normal astrocytes under the effects of NDGA. The purpose is to find evidence of this acid's influence on normal cells/tissue. The finding in the current work can lead to a possible non-invasive treatment for brain cancer. Thus, in the following chapters, we are going to describe the experimental methodology and the associated theory behind vibrational spectroscopy, which is the main technique employed. This will be followed by results and concluding remarks. Possible future steps that can be done as a continuation to the project will also be discussed.

Chapter 2: Experimental Methodology

In vibrational spectroscopy, the main techniques for the detection of vibrations in molecules rely on the phenomena of infrared absorption and Raman scattering. These techniques provide solutions to demanding analytical problems. They are primarily used to obtain structural information and/or configuration chemically and physically. Recognizing substances from the vibrational structure/patterns or «fingerprint» and establishing the quantity of a substance in a sample have applications spanning numerous research fields. Several physical forms of samples that can be examined, such as solid, liquid, and gaseous states. Sample degradation and fluorescence were problems that prevented Raman scattering from being a more commonly used technique compared to infrared absorption. However, new advances in technology and instrumentation improved the performance of currently employed equipment in physio-chemical analyses and reduced such issues. These technological improvements in sensitivity and reliability, in conjunction with the capacity of Raman spectroscopy to examine aqueous solutions or samples without much need for previous preparation (just placed in glass containers), contributed to a quick expansion in the applications of Raman spectroscopy [19].

In this chapter, we focus on Raman spectroscopy since it is the technique used in this project. Larkin defined Raman spectroscopy as a two-photon inelastic light scattering event [20]. In the following sections of this chapter, we will go more in-depth about this technique and briefly discuss its history, the basic theory behind Raman spectroscopy, the equipment used, and the experimental setup.

2.1 Raman Spectroscopy Brief History

The origin of Raman spectroscopy dates back to the 1920s when the Austrian theoretical physicist, Adolf Smekal, postulated the phenomenon of inelastic scattering of light in 1923. However, it was until 1928 that the phenomenon was observed experimentally by the Indian physicists, Sir C. V. Raman, and K. S. Krishnan. In recognition of his discovery, Raman was awarded the Nobel Prize in 1930 [19,21].

Ferraro, Nakamoto, and Brown (2003) mentioned that Sir Raman used in his work sunlight as the source, a telescope as the collector, and his eyes as the detector [22]. The molecules were excited with filtered sunlight, and the spectrum was recorded on photographic plates. Capturing the spectrum of a breaker containing about 600 ml of pure liquid took about 24 hours. Thus, at that time, Raman spectroscopy was used exclusively in specialized research labs, in addition to the method being regarded as an oddity [23]. However, we can say the discovery of this phenomenon was impressive.

The difference between the use of infrared absorption and Raman scattering was notorious. The complexity in the instrumentation of Raman spectroscopy, the measurement processes, and the alignment were the reasons why this technique remained limited to specialized laboratories. Thus, infrared spectroscopy remained relevant and considered user-friendly until continuous improvements in Raman spectroscopy start gaining scientific and technological ground. It was in the 1960s when research employing Raman spectroscopy made great progress because of the introduction of new lasers. However, there was still room for more improvements. Additional progress was made in the 1980s with the advent of new instrumentation, such as the charged-coupled device sensors (CCD), holographic filters, Raman microscopy, and Fourier-transform Raman spectroscopy. Nowadays, these techniques are used not only in specialized laboratories,

but also in research places in academia and industries. These continuous improvements made the technique reliable, accessible, and appreciated in the research field [23].

2.2 Raman Spectroscopy Theoretical Background

Light is categorized as electromagnetic radiation, which is a combination of alternating electric and magnetic fields. The motion of these fields is described as a continuous sinusoidal wave, where the electric component is perpendicular to the magnetic component, and they are propagated in the same direction (Figure 2.1 shows this description) [20].

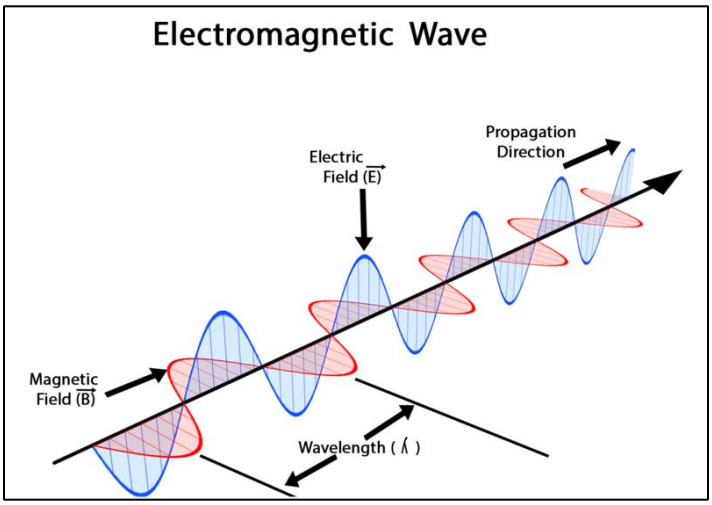

Figure 2.1. Electromagnetic wave. [24]

In studying Raman spectroscopy, the magnetic field can be neglected. Thus, we will consider the electric field at a time *t* given by the following expression:

$$E = E_0 \cos(2\pi\nu t) \tag{2.1}$$

where ν is the frequency. The important parameters that describe radiation are frequency (ν), wavelength (λ), and wavenumber ($\tilde{\nu}$). In spectroscopy, we are interested in the radiation's

interaction with the molecule's states, which is described often in terms of energy. The parameters mentioned before are related to energy by the following relations: [19,20,22]

$$\nu = \frac{\Delta E_n}{h} \tag{2.2}$$

$$\lambda = \frac{c}{\nu} \tag{2.3}$$

$$\tilde{\nu} = \frac{\nu}{c} \tag{2.4}$$

In Raman spectroscopy, light-matter interaction is given in an off-resonance way, where the light causes polarization in the molecule. In other words, when the interaction between the light and molecule occurs, the light distorts the cloud of electrons that are around the nuclei and forms a temporary, unstable state called «virtual state» [19,20].

In vibrational spectroscopy, the energy changes that are detected are those necessary to trigger nuclear motion. We know that electrons are relatively light. Therefore, photons are going to be scattered with very small changes in the frequency if the only event involved in the scattering process is the electron cloud distortion. This process is the dominant one and is an elastic scattering. When we speak about molecules this scattering is commonly referred to as «Rayleigh scattering». Now, if in the scattering process a nuclear motion is produced, energy is going to be transferred. This energy transfer can happen in the following two cases: the incident photon can pass the energy to the molecule, or the molecule can pass the energy to the scattered photon. Here, the energies of the scattered and incident photons are different by a vibrational unit. This process is an inelastic scattering and is known as «Raman scattering». In this process, only one photon is Raman scattered in every 10^6 — 10^8 photons that scatter. Therefore, is considered a weak —but not an insensitive— process [19].

At ambient temperature, many of the molecules are found in the vibrational level with the lowest energy. We mentioned before that the virtual state is created when light causes polarization

in the molecule and the frequency of the light source is the frequency that determines the energy of this state. Since most of the photons are Rayleigh scattered, this process will be the most intense. In this basic process, the light comes back to the same energy state; this occurs because the energy remains the same, that is, there is not any change in the energy [19]. In the Raman scattering process, two cases usually occur. In one case, the molecule transitions from the ground vibrational state to the first excited state. This is called the *Stokes Raman scattering*. However, since the excited vibrational states could be already occupied —at higher temperatures— the transition could be from the first excited state to the ground state. This is the *anti-Stokes Raman scattering* [21]. These basic processes that occur for one vibration are shown in Figure 2.2:

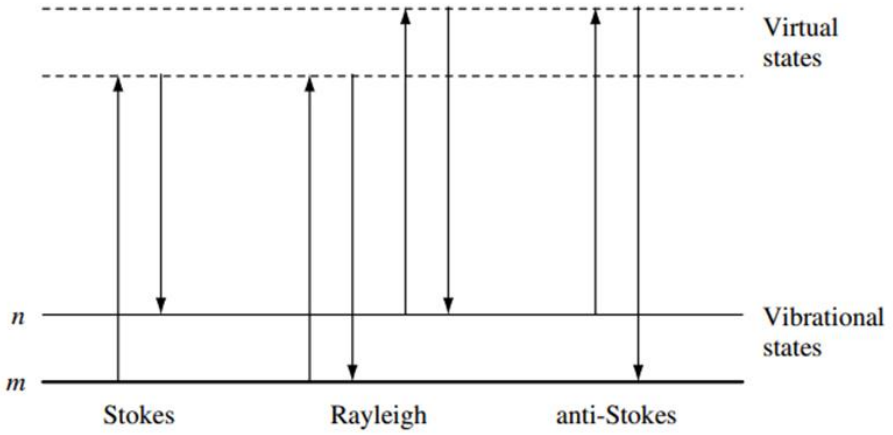

Figure 2.2. Rayleigh and Raman scattering processes. The ground vibrational state is represented by m and the excited vibrational state is represented by n. [19]

The upward arrows represent the energetic transition from the ground state to the exited state and the downward arrows represent the scattered energy, which can be lower (*Stokes Raman scattering*) or higher (*anti-Stokes Raman scattering*). These energies are larger than the energy of a vibration. It is also important to mention that in the Stokes process there is energy absorption by the molecule, and in the anti-Stokes process, energy is transferred to the scattered photon.

Furthermore, the relative intensities of these processes depend on the fraction of molecules in each vibrational state [19]. We can calculate this fraction with the Boltzmann distribution equation:

$$\frac{N_1}{N_0} = e^{-\frac{\Delta\varepsilon}{kT}} \tag{2.5}$$

where N_1 is the number of molecules in the first excited state, N_0 is the number of molecules in the ground state, $\Delta\varepsilon$ is the difference of the ground state and first excited state energies, k is the Boltzmann's constant, and T is the temperature of the sample [21].

At ambient temperature, the number of molecules in an excited vibrational state, excluding those of significantly low energy, will be small. As a result, the Stokes scattering will be stronger in comparison to the anti-Stokes scattering. As the vibration frequency rises, due to a reduction in the population or fraction of excited vibrational states, the anti-Stokes scattering will get even weaker. On the other hand, when the temperature rises, the anti-Stokes scattering will become more prominent than the Stokes scattering [19].

While experiments are mostly performed in the Stokes energetic region, anti-Stokes scattering is often favored to prevent fluorescence. Since fluorescence interference occurs at a lower energy than that of the excitation frequency, Raman scattering is commonly set down just on this low energy side [19]. However, Stokes scattering is preferred due to a higher yield. Furthermore, the temperature of a sample can also be measured by comparing the anti-Stokes and Stokes intensities of the Raman spectra [21].

2.2.1 Classical Approach

As part of the theoretical background, we mentioned light as electromagnetic radiation. However, the magnetic field is commonly neglected at analyzing Raman spectroscopy. Let us

recall equation (2.1), which is the expression for the electric field. In the classical aspect of the Raman theoretical background, we are going to start by analyzing a diatomic molecule.

An electrical dipole moment is induced when the molecule is affected by a beam of light, namely when interacts with the electrical field. The expression for this dipole moment is given by:

$$P = \alpha E \tag{2.6}$$

where E is expressed by equation (2.1) and α is the molecule polarizability, which is a tensor that depends on the normal coordinate of the molecule. Therefore, we can express the polarizability in a Taylor series expression as follows:

$$\alpha = \alpha_0 + \sum_i \left(\frac{\partial \alpha}{\partial Q_i}\right)_0 Q_i + \frac{1}{2}\sum_{i,j}\left(\frac{\partial^2 \alpha}{\partial Q_i \partial Q_j}\right)_0 Q_i Q_j + \cdots \tag{2.7}$$

where Q is the normal coordinate in the i^{th} and j^{th} normal vibration.

Let us consider the normal vibrations as being completely independent. Into a first approximation, only the first two terms in equation (2.7) become important. Therefore, the expression for a k^{th} normal vibration can be simplified as:

$$\alpha_k = \alpha_0 + \alpha'_k Q_k \tag{2.8}$$

with the apostrophe representing the derivative.

Thus, in a first approximation, we can say that the oscillations of the normal coordinates behave as in the case of a harmonic oscillator. The expression for the normal coordinate is:

$$Q_k = Q_{k0}\, cos(2\pi \nu_k t) \tag{2.9}$$

where Q_{k0} is the amplitude of the normal coordinate. Now, substituting equation (2.9) in the equation (2.8) we have:

$$\alpha_k = \alpha_0 + \alpha'_k Q_{k0} cos(2\pi \nu_k t) \tag{2.10}$$

In addition to the normal coordinates oscillating as a harmonic oscillator, we are going to assume that the polarizability tensor also behaves as a harmonic oscillator, with ν_k being the frequency of the oscillation.

We can substitute the equation (2.10) and (2.1) in the expression (2.6), considering that $\alpha \equiv \alpha_k$. Thus, we have:

$$P = \alpha_0 E_0 cos(2\pi\nu t) + \alpha'_k E_0 Q_{k0} cos(2\pi\nu t) cos(2\pi\nu_k t) \tag{2.11}$$

Using the trigonometrical property of *cosAcosB*, we obtain:

$$P = \alpha_0 E_0 cos(2\pi\nu t) + \frac{1}{2}\alpha'_k E_0 Q_{k0}\, cos[2\pi(\nu + \nu_k)t] \tag{2.12}$$

$$+ \frac{1}{2}\alpha'_k E_0 Q_{k0}\, cos[2\pi(\nu - \nu_k)t]$$

Analyzing this latter equation, we can conclude that the electrical dipole moment is dependent on the vibrational frequencies of both the incident beam and the molecule. Therefore, we can rewrite this expression as a function of frequency as follows [23]:

$$P = P(\nu) + P(\nu + \nu_0) + P(\nu - \nu_0) \tag{2.13}$$

where the first term represents the elastic scattering of the light, also known as the Rayleigh scattering. This implies that the frequency in this term of the dipole moment is the same as the radiation frequency [23]. Consequently, the energies of both, the first term of the dipole moment and the electromagnetic radiation will also be the same. The second and third terms in equation (2.13) are corresponding to inelastic scattering [23]. They are the ones correlated with the Raman scattering. The dipole moment in the second term is dependent on the sum of frequencies. This means that the resultant frequency is going to be larger than the frequency of the incident radiation. A similar result is expected for energies. This type of Raman scattering is associate with the anti-Stokes scattering mentioned previously. Since the third term is dependent on the subtraction of

frequencies, it leads us to the conclusion that the energy would be lower than the energy of the incident beam. This corresponds to the Stokes scattering [23].

The Raman spectrum of mineral realgar (As_4S_4) is presented in Figure 2.3 below as an example, with all of the three types of scattering clearly labeled.

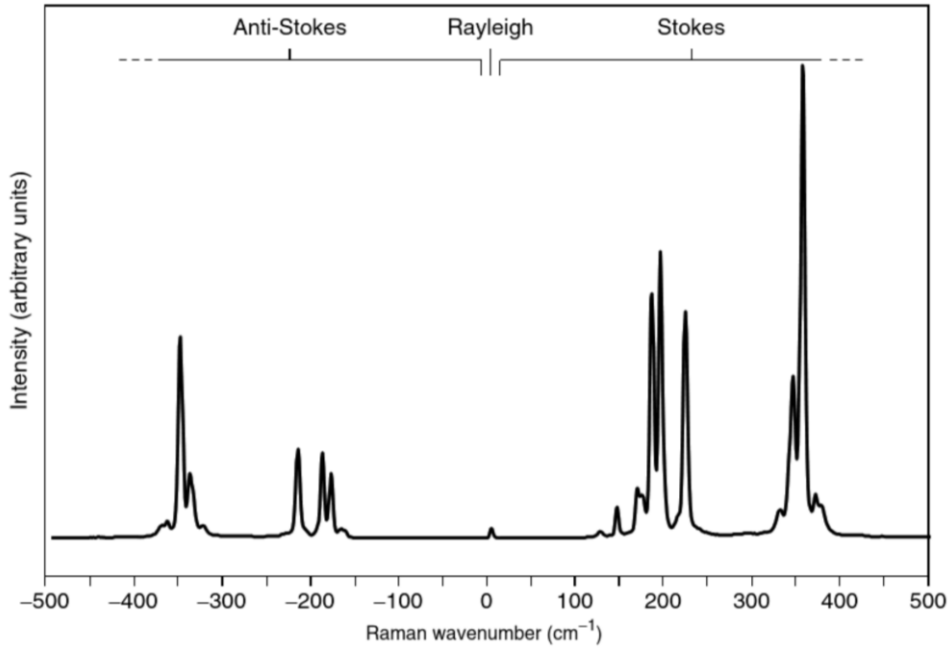

Figure 2.3. Raman spectra for As_4S_4. [23]

2.3 Confocal Raman Microscopy

It is widely believed that Dutch eyeglass manufacturer Hans Janssen and his son Zacharias were the first to combine numerous lenses to create an optical microscope around the end of the 16th century. The magnifying properties of water filled glass spheres were known over 2000 years ago, when the philosopher Seneca described them. However, even though many experts and researchers knew about the use of convex lenses, it took more than a thousand years to make improvements and be able to construct an optical microscope by combining multiple lenses. Ernst

Abbe, a professor of physics in Jena, Germany, established his optical image creation theory in 1873, which laid the groundwork for understanding the physics behind the optical microscope. These improvements in the optical microscopy enables others, such as the diffraction-limited optical microscopy that appeared through the years. The developments in this technique were widely notorious in the 20th century, with the appearance of new imaging techniques. However, the most important was and still is the confocal microscopy, which was set as a standard technique at the end of the 1980's decade [25].

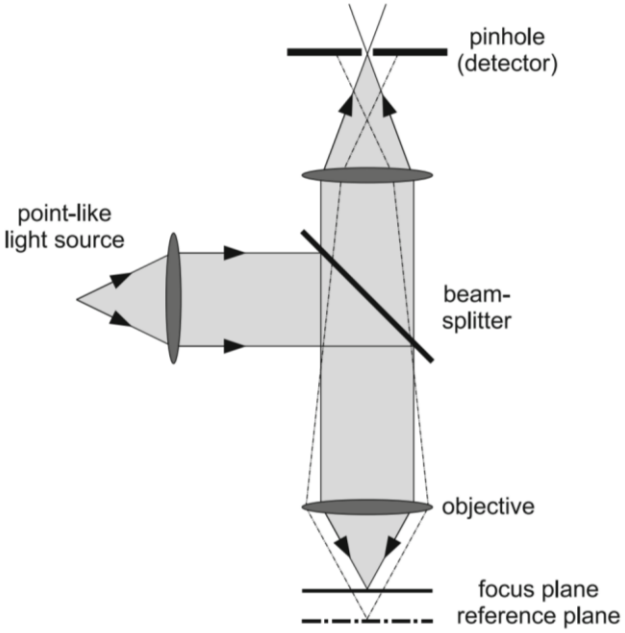

Figure 2.4. The main setup for a confocal microscope. [25]

In confocal microscopy, a tiny aperture found in front of the detector captures the image of a source of light, specifically a point-like type of source —like a laser— that is directed onto the sample. The illuminating area is confocal with the aperture since it is placed in the microscope's image plane. The confocal microscope is widely complex compared to the traditional optical microscope. It can generate an image of a sample only by scanning the sample — by exciting point

by point and line by line a selected area. However, the complexity of the confocal microscope is of no concern compared to its great advantage — the recorded picture is unaffected by the dispersed light from above or below the focus point. This is because the light observed is limited to a narrow region surrounding the focus point. Another important advantage in confocal microscopy is the depth resolution and the significantly improved picture contrast thanks to the elimination of deviated light [25].

The technique's advantages have been further developed to confocal Raman microscopy, which combines development through the years in both, the microscopy and the Raman technique. These improvements were usually done to satisfy the needs and demands of modern research. Every time disadvantages were found the experts tried to solve them; therefore, better equipment was introduced. For example, historically, the combination between a Raman spectrometer and an optical microscope was done around the 1990's decade. This combination resulted in introduction of micro-Raman spectroscopy. With this technique, measurements of small parts of samples (of a few square micrometers) were successfully obtained. In this context is worth mentioning that a highly intense laser focused on a small area can burn a sample. To avoid this unwanted consequence, scientists were recommended to be thoroughly careful during such measurements [25].

One of the disadvantages of the Raman spectroscopy is the interference of fluorescence, which can be a dominant effect. The Raman scattering is normally weak; therefore, the fluorescence efficiency tends to be much higher than the Raman interaction efficiency, causing most of the times only fluorescence to be detected instead of the Raman signal. Reduction of the fluorescence interference is critical. There are two ways to achieve this. Using a light beam whose wavelength has a value where fluorescence cannot be encountered or limiting the detection

volume. The first option is not always possible. Therefore, the only way is by volume reduction. This can be achieved by employing a confocal detection setup. Since the arrangement restricts the detection of the fluorescence signal, Raman images may be produced in instances where fluorescence was dominating in measurements using different techniques [25]. In the *Confocal Raman Microscopy* book is also mentioned that the confocal detection principle restricts not only the detected light to the focal plane, but it also enables the study of transparent samples in three dimensions. In addition, it allows the performance of an optical cross section without having to divide the sample in halves. Only a confocal arrangement allows for differentiating between the signal from the sample from the one corresponding to the background produced by the substrate. This effect becomes important when the sample is a thin layer placed on top of a supporting surface, since there are cases where the Raman signal from the sample is smaller than the one produced by the surface. These smaller signals are hardly visible and thus, more difficult to analyze in a non-confocal technique [25].

We can conclude that even if the non-confocal techniques have their own advantages, the confocal Raman microscopy technique brings much better benefits. In highlighting some of them — better analysis in smaller Raman signals compared to that of the surface the sample is placed in, reduction of fluorescence encountered in some samples, focus in microscopic areas enabling the measurements of microscopic samples. In general, the confocal Raman microscopy technique has shown to be the most flexible method for achieving the highest spatial resolution and noise suppression [25].

2.4 Experimental Set-Up

Commonly, the structure of a Raman spectrometer has four main components as the base setup. These components are: an excitation source, a light collector system, a monochromator, and a detector. When the Raman spectrometer was first introduced, the excitation source used to be a mercury lamp. Nowadays this light source is a laser. Similar to the light source, the human eye was used as the detector, until technologically was replaced by photomultiplier tubes (PTM) and charged-coupled device (CCD) sensors [26].

These Raman equipment components by working together provide us with the structural information (fingerprint) of the samples. However, other components are needed to be able to measure small spots in a microscopic sample. These new components along with those of the Raman spectrometer form a confocal Raman microscope. Figure 2.5 shows schematically the components of such microscope [26].

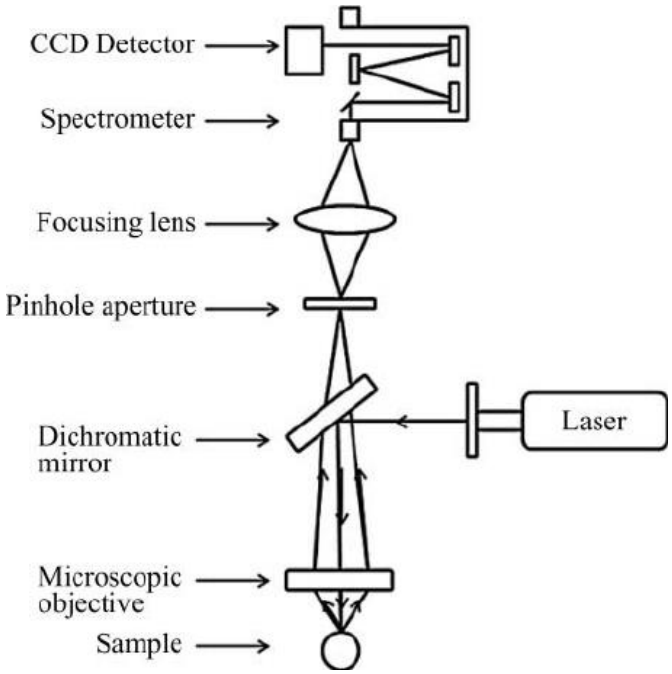

Figure 2.5. Confocal Raman microscope schematic. [26]

Zhu, X. et al. mention in an article that in order to prevent any out-of-focus light that comes from beyond the sampling volume, the laser light should be directed on the sample using an objective lens of a microscope. In this case, the backscattered Raman signal will be refocused by a pinhole aperture. A CCD camera disperses the filtered Raman signals sent to the spectrometer, thus, creating spectra [26]. This gives us a brief picture of the components in the confocal Raman microscope and how they work together. A structure of the equipment employed in the current measurements is described in more depth below.

The components in the different equipment can vary. The instrumentation in the Optical Spectroscopy and Microscopy laboratory at The University of Texas at El Paso is an *alpha 300 RAS* WITec system. The letters RAS imply that the system is modular; they correspond to each technique available employing this equipment. The letter "R" corresponds to the confocal Raman microscopy, the letter "A" to the atomic force microscopy (AFM), and the letter "S" to the scanning near-field optical microscopy (SNOM) [27]. Only the confocal Raman was used to acquire the data. Thus, this part of the system is presented throughout in what follows.

The WITec system couples a high-efficiency Raman spectrometer to a confocal microscope of high resolution. Not only can a Raman signal of materials be obtained with this pairing, but it can also be combined with a lateral resolution in the sub-micrometer range. A detailed information of the chemical structure of the materials analyzed can be obtained from the recorded spectra. In addition, microscopically, a resolution down to 220 nm may be achieved using the green light laser source [28]. The current system consists of an upper microscope and uses an Nd:YAG laser at 532 nm as the light source excitation.

Figure 2.6 shows the upper microscope schematic and its standard components of the alpha 300 equipment [27]. In this schematic, we find components in a dark color and a light color. A

color-coding is done to distinguish between the common parts used also in AFM or SNOM techniques besides the parts that are specific to the confocal Raman [27]. Thus, in the following list that is adapted from the user manual [27], the names of the components corresponding specifically to the confocal Raman techniques are in dark letters. The purpose of each component is also presented below.

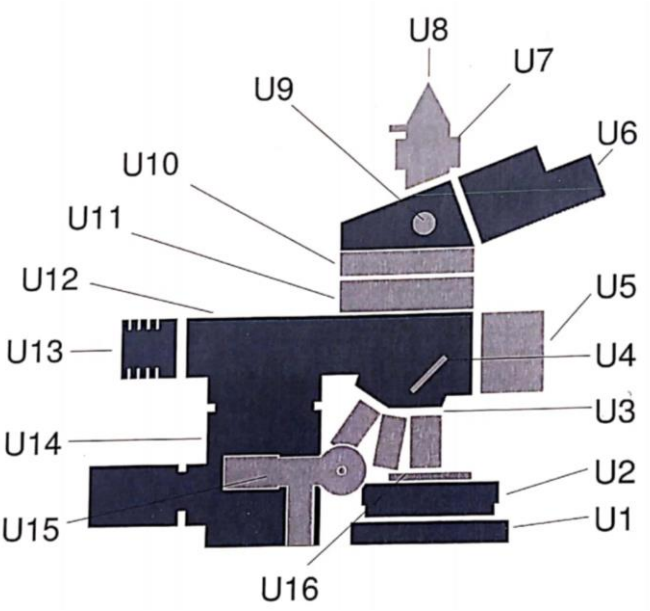

U1 — XY positioner

U2 — Scan stage

U3 — Objective turret with objectives

U4 — Dichroic mirror

U5 — Beam deflection unit

U6 — Binocular tube with ocular camera

U9 — Pushrod

U10 — Filter slider unit

U11 — Laser coupling unit optical input

U12 — Microscope body with Köhler illumination

U13 — Light source

U14 — Microscope Z stage with stepper motor

U7 — Filter holder for reflection mode measurements

U8 — Fiber coupling unit optical output

U15 — Near-field reflection mode detection unit

U16 — Heating stage

Figure 2.6. The upper microscope schematic. [27]

The **XY positioner** allows us to align the sample in the X and Y directions with smooth and linear movement. The positioner is found under the **scan stage,** which is a piezoelectric driven 3-axis flexure stage. This stage is used to scan the sample for all operation modes. The system is equipped with three **objectives:** of 20x, 50x, and 100x magnification. Each of the objectives collects light that is sent to the **ocular camera** or the detector with the help of a sliding prism controlled by a **pushrode**; the ocular camera moves through one of the **binocular tubes** and the binocular tubes give a vertical image. The ocular camera is used instead of ocular eyepieces due to safety reasons regarding the laser intensity. The **fiber coupling unit optical output** allows us to optimize the optical performance. In Raman experiments, suppressing the Rayleigh scattering signal is desirable. To achieve this, a **filter slider unit** is used along with a filter. To focus the sample, a highly bright white light LED (the **light source** component) along with a diffuser is first used. For such task, a **Microscope Z stage with stepper motor** is used to move the microscope in the Z axis [27].

All of these features of the confocal Raman microscope give us a wide variety of operation modes, such as: [28]

- Collection of Raman spectra at selected sample areas, also known as single spectra.
- Collection of time series of single spectra.

- Raman spectral imaging.
- Collection of Raman spectra along a selected line, also known as line spectrum.

As concluding remarks, this chapter gives us a better understanding of the Raman spectroscopy and confocal Raman functionality and fundamentals. We saw how the techniques have been improved through the years until we have the instrumentation and technology of nowadays. However, it is important to note that even if old techniques are still used because of their own advantages, the newly developed techniques bring more and widely notorious benefits to our experimental performance. The understanding of these advantages, the theory behind the development of an equipment and of its functionality is critical in allowing us to choose what is better for our study purposes and for the project directions.

Chapter 3: Results and Discussion

Glioblastoma (GBM) is the most malignant brain tumor, with an average survival rate for patients of 15 months. Current treatment methods are highly invasive and even though physicians and scientists do their best to have a better outcome for patients, the prognosis and survival rate remain bad. Nowadays, finding better alternatives for cancer treatment is one of the main focuses for scientists working in the biological and health area [12].

Our previous research consisted in analyzing glioblastoma (GBM) cells under the effects of nordihydroguaiaretic acid (NDGA) chemical extract from *Larrea Tridentata*, with the hypothesis that this could lead to a potential brain cancer treatment. This plant, which has been widely used in traditional medicine, is known to have therapeutic effects for several diseases such as urinary tract infections, kidney stones, diabetes, and cancer [17,18]. For our research, we used confocal Raman microscopy to analyze the samples. We found promising results that will be further discussed in this chapter.

Having the results for glioblastoma multiforme and knowing that current cancer treatments are invasive, a new question is: “What effects has NDGA on normal cells?” Thus, to seek answers, we performed experiments on normal astrocytes under the effects of NDGA. In the following sections, we will discuss our Raman results for normal astrocytes under the effects of NDGA. However, for a needed comparison, we will start with the previous findings of the compound’s influence on GBM.

3.1 Sample Preparation and Instruments Configuration

In these experiments, samples from the Mayo Clinic's National patient-derived xenografts repository were used. The sample preparation followed the standard procedure of cells' fixing on a microscope glass slide. The cells were plated in culture flasks, washed with phosphate buffer and detached from the flask. Fetal bovine serum, high glucose, and penicillin-streptomycin were added into the flask, followed by centrifugation of the mixture containing the isolated cells. After this procedure, the cells were incubated for 24 hours in a 100 μM NDGA concentration and for 4 hours in a 250 μM NDGA concentration. Finally, the cells were fixed on a plain microscope glass slide using 4% paraformaldehyde and washed five times with PBS and doubly distilled water. They were air dried at room temperature [29].

An alpha 300 RAS WITec modular system was employed in the current confocal Raman measurements. The excitation of an Nd:YAG laser at 532 nm, a 50X objective lens with a numerical aperture of 0.75 were used. Sample damage was avoided by maintaining the average laser power around 3mW. The Raman mapping images were obtained by collecting arrays of 150 x 150 Raman spectra with an integration time of 500 ms [29].

3.2 NDGA Therapeutic Effects on Glioblastoma Multiforme

The confocal Raman microscopic experiments performed on GBM malignant cell line include besides the control sample, which consisted of untreated glioblastoma cells, two NDGA-treated GBM cells with two different concentrations, 100 μM and 250 μM.

In Figure 3.1 we present the summary of these results that demonstrates NDGA's therapeutic effect on glioblastoma multiforme for both these concentrations. It can be observed that a high dosage of NDGA has a similar outcome as a quasi-chemotherapy approach. This remark

is supported by the membrane and other structural cell damage for treatment with a 250 µM concentration. On the other hand, a treatment with repetitive, smaller NDGA dosages over a longer time is recommended, as explained below.

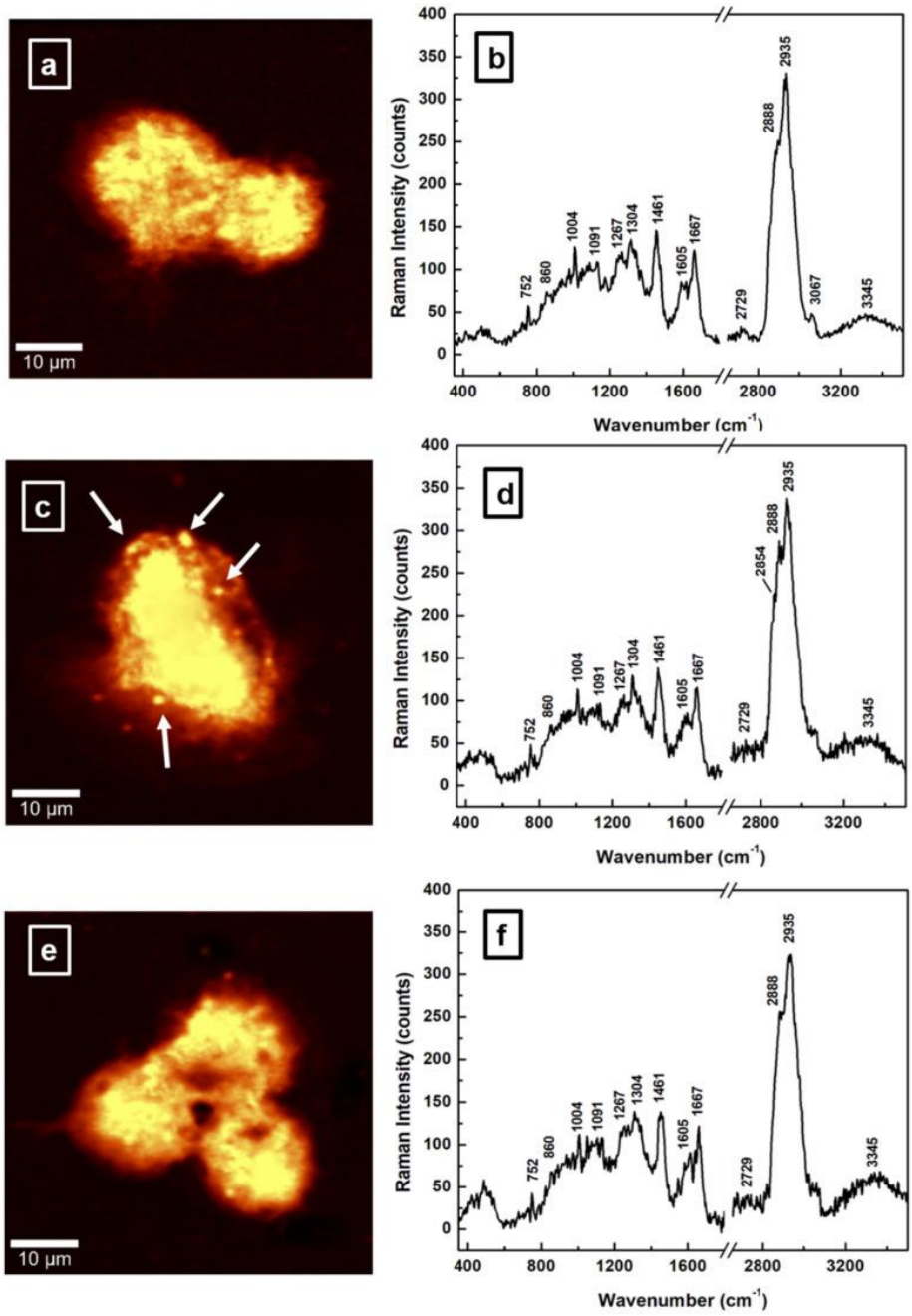

Figure 3.1. Confocal Raman mapping and integrated spectra of untreated (a-b), 100 µM NDGA-treated for 24 h (c-d) and 250 µM NDGA treated for 4 h (e-f) GBM cells. [29]

In comparing the integrated spectra of the control sample (untreated GBM) with those treated with two different concentrations, we first focus on 2888 cm^{-1} and 2935 cm^{-1} Raman peaks at the higher frequency spectral region. They correspond to the lipid (the 2888 cm^{-1} signature) to the protein (the 2935 cm^{-1} vibration) changing bio-ratio. In many types of cancers, it was found that an abnormal lipid-protein metabolism takes place [29]. Therefore, focusing on this region is crucial. In Figure 3.1, we can observe a decrease in this protein/lipid intensity ratio for the 100 μM concentration, while for the 250 μM it increases. It is expected that, for normal, healthy tissue, this ratio is low. Therefore, we can conclude that NDGA treatment has a beneficial effect at lower concentrations. The presence of lipid droplets is pointed with white arrows for treatment with 100 μM NDGA concentration, showing that the compound is acting on the lipid-to-protein metabolism [29].

Another region of interest is 1000 cm^{-1} to 1300 cm^{-1}. The 1004 cm^{-1}, which corresponds to the phenylalanine biomarker, shows an increase in its intensity at 250 μM NDGA concentration. This increase, which typically occurs in cancerigenic samples, is now an indication of damaged cells at this high-toxicity concentration. Opposite to this statement, there is a decrease in the intensity of this peak when a 100 μM NDGA concentration is used. Once again, this is evidence of NDGA's benefic effects on GBM at lower concentrations and the effect of the compound in scavenging the ROS (reactive oxygen species) species [29].

3.3 Normal Astrocytes Under the Effect of NDGA's Treatment

Although we found evidence that NDGA has some therapeutic effects for glioblastoma multiforme at lower concentrations, just as any other treatment method side effects are of concern due to the potential toxicity of the compound at high concentrations. As beneficial as it can be to

treat or prevent certain diseases, an uncontrolled intake of this phenolic lignan can damage other organs [17]. Therefore, to find a potential non-invasive brain cancer treatment, a detailed study of NDGA's effects on normal tissue is also important. Confocal Raman microscopic experiments on normal astrocytes under the effects of NDGA are the focus of this research and are discussed in what follows.

3.3.1 Raman Microscopic Results of Untreated Astrocytes

An investigation of untreated astrocytes was first performed to acquire the needed control sample results for future comparison with those after NDGA administration. To overcome any sample inhomogeneity several Raman mappings were performed at different locations on different samples. Some of the selected confocal Raman images and their associated integrated spectra (averages over 22,500 spectra per image) are presented in Figure 3.2. The spectroscopic results were processed using OriginPro for background subtraction and normalization to the 2935 cm^{-1} vibrational line intensity.

While the integrated spectra for each image show relatively similar features, there are some minuscule discrepancies. For a better understanding of the analysis of these Raman changes, tentative assignments of the bands according to literature is summarized in Table 3.1. These tentative assignments will be used further for analyzing and identifying changes between the control sample (normal astrocytes) and the results after NDGA cell treatment with two different concentrations. We will put special attention to the Raman vibrational bands attributed to phenylalanine, lipids, and proteins. The reason behind this is that these signatures have a significant contribution in discriminating between normal tissue/cells and GBM. Besides

identifying cell malignancy or abnormal behavior they also provided insights into the NDGA mechanism of action.

Table 3.1. Raman shifts and their tentative assignment. [29,30]

Raman shift (cm^{-1})	**Tentative assignment**
752	DNA, symmetric breathing of tryptophan, cytochrome c
860	C-C stretch proline, tyrosine, glycogen
1004	C-C phenylalanine ring breathing
1267	Amide III, fatty acids
1461	Lipid (CH_2), protein
1667	Amide I
2888	CH_2 asymmetric stretch in lipids
2935	CH_3 symmetric stretch in proteins

From the confocal Raman images presented in Figure 3.2, the middle one reveals the presence of additional tissue surrounding the cell. A closer look at the intensity of 2888 cm^{-1} Raman signature attributed to lipids shows a slight increase compared with the first and the third one. This statement is confirmed by the presence of lipid droplets observed in this image.

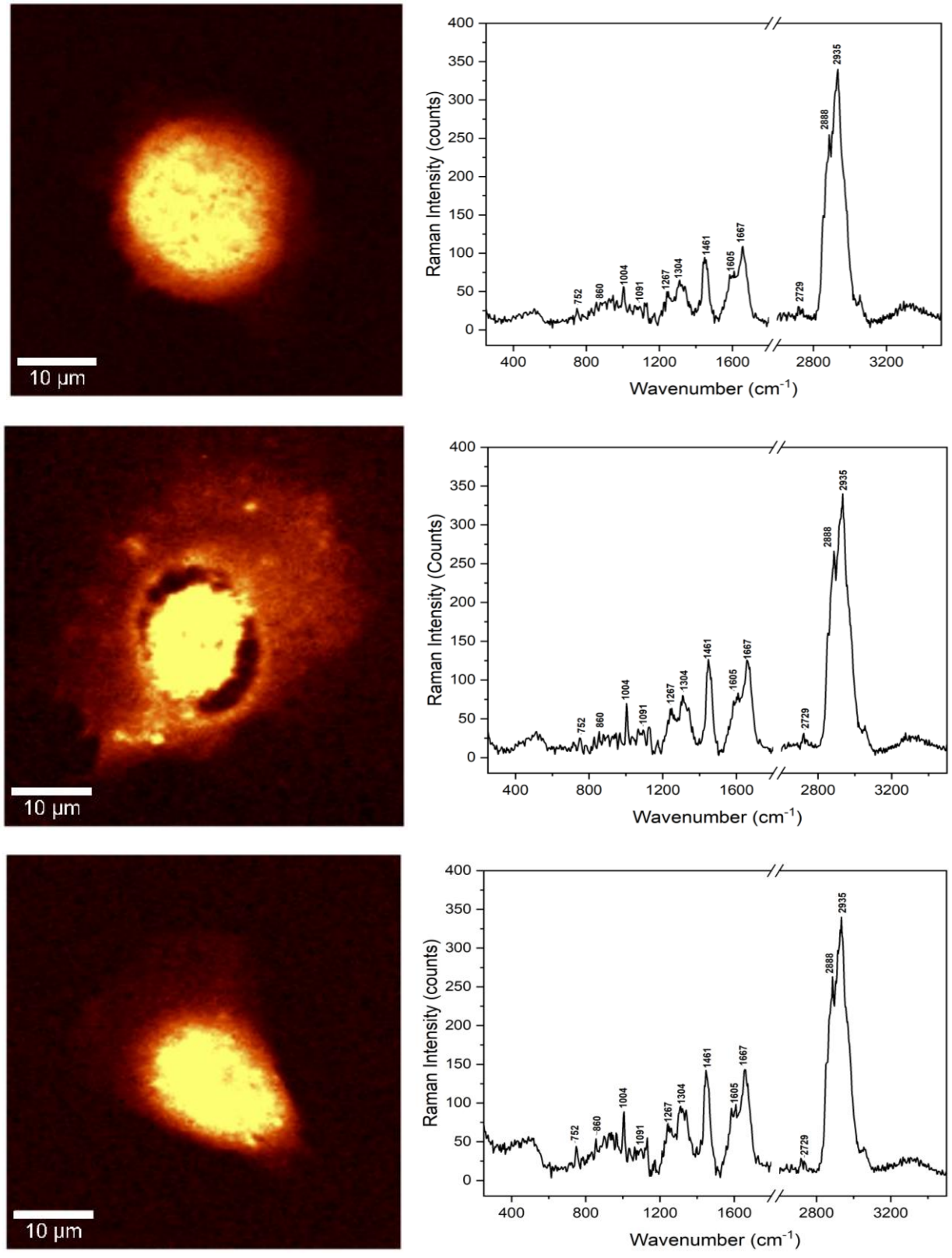

Figure 3.2. Confocal Raman mapping and spectra of normal astrocyte cells.

In addition to these three confocal Raman measurements of different astrocytes other two cell measurements were considered, for a total number of five, in obtaining the average integrated Raman spectrum presented in Figure 3.3. This spectrum is going to be used for the final comparison between the control and the samples treated with two different concentrations.

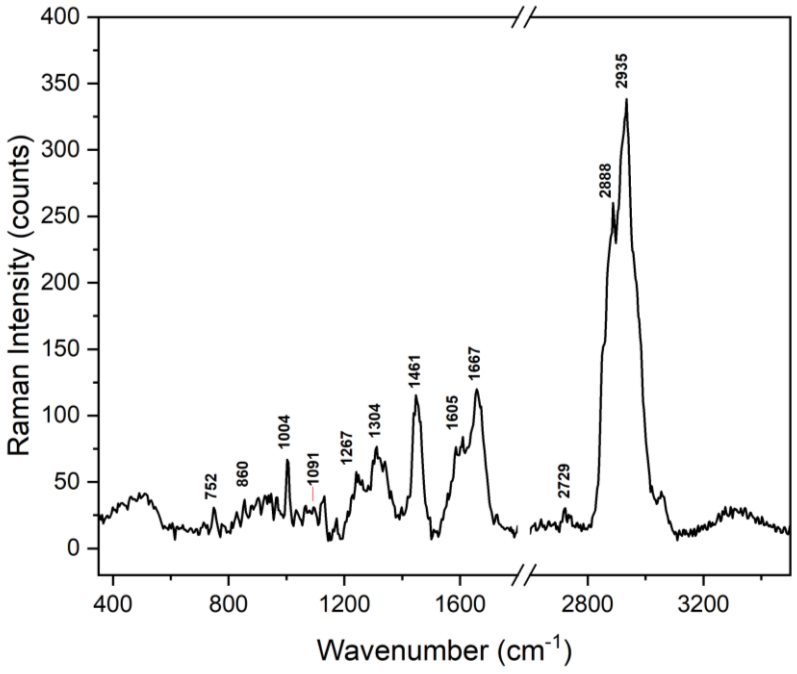

Figure 3.3. Average integrated spectra for untreated astrocyte cells.

3.3.2 100 µM NDGA-Treated Astrocytes

Several samples of astrocytes treated with an NDGA concentration of 100 µM for 24 hours were measured and analyzed. Similar to the untreated astrocytes (control samples), we select five different cell measurements. Figure 3.4 is a representation of three of these measurements.

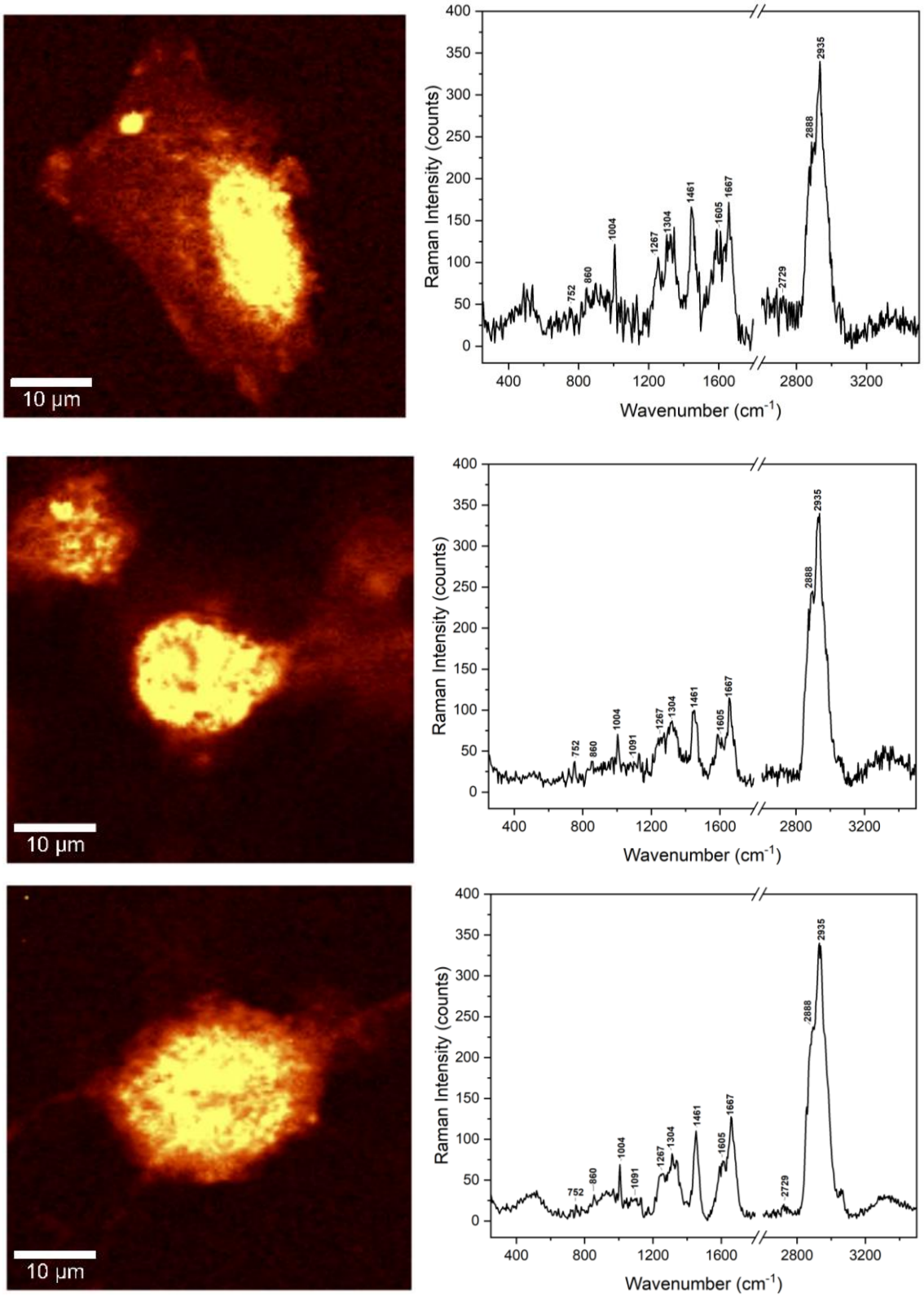

Figure 3.4. Confocal Raman mapping and spectra of 100 μM treated cells.

If we were to compare these individual results with the ones reported in Figure 3.2, we can already observe slight differences. For instance, an increase in the intensities of 1004 cm^{-1} wavenumber and a very likely increase in the protein-to-lipid ratio (the ratio of the intensities of peaks at 2935 cm^{-1} and 2888 cm^{-1}) can be depicted. The average of all five integrated spectra is presented in Figure 3.5. This average spectrum will be used for further comparison between the samples.

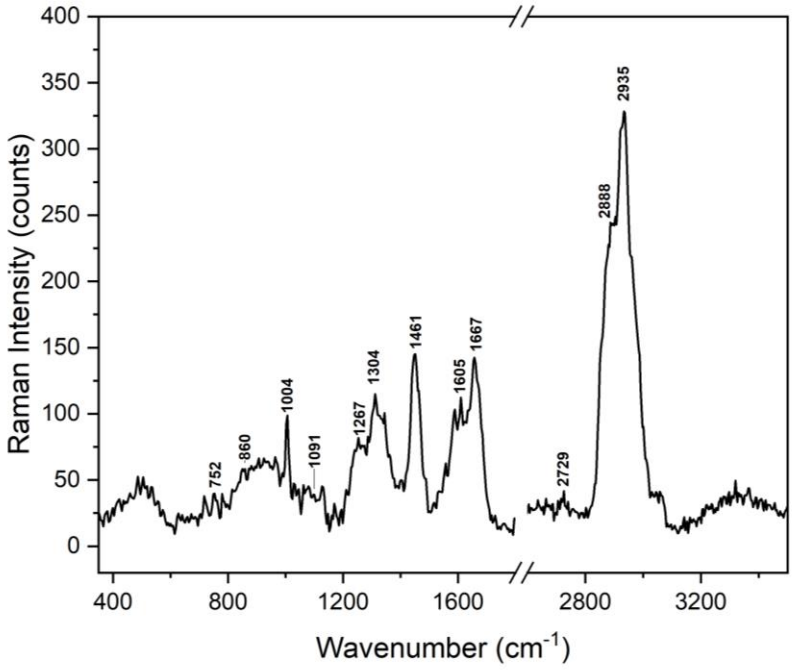

Figure 3.5. Average integrated spectra of 100 µM NDGA-treated cells.

3.3.3 250 µM NDGA-Treated Astrocytes

Finally, we repeated the confocal Raman experiments for astrocytes treated with a 250 µM NDGA concentration. For consistency purposes, we selected measurements of five different cells (spectra and confocal mapping images), with only three presented in Figure 3.6.

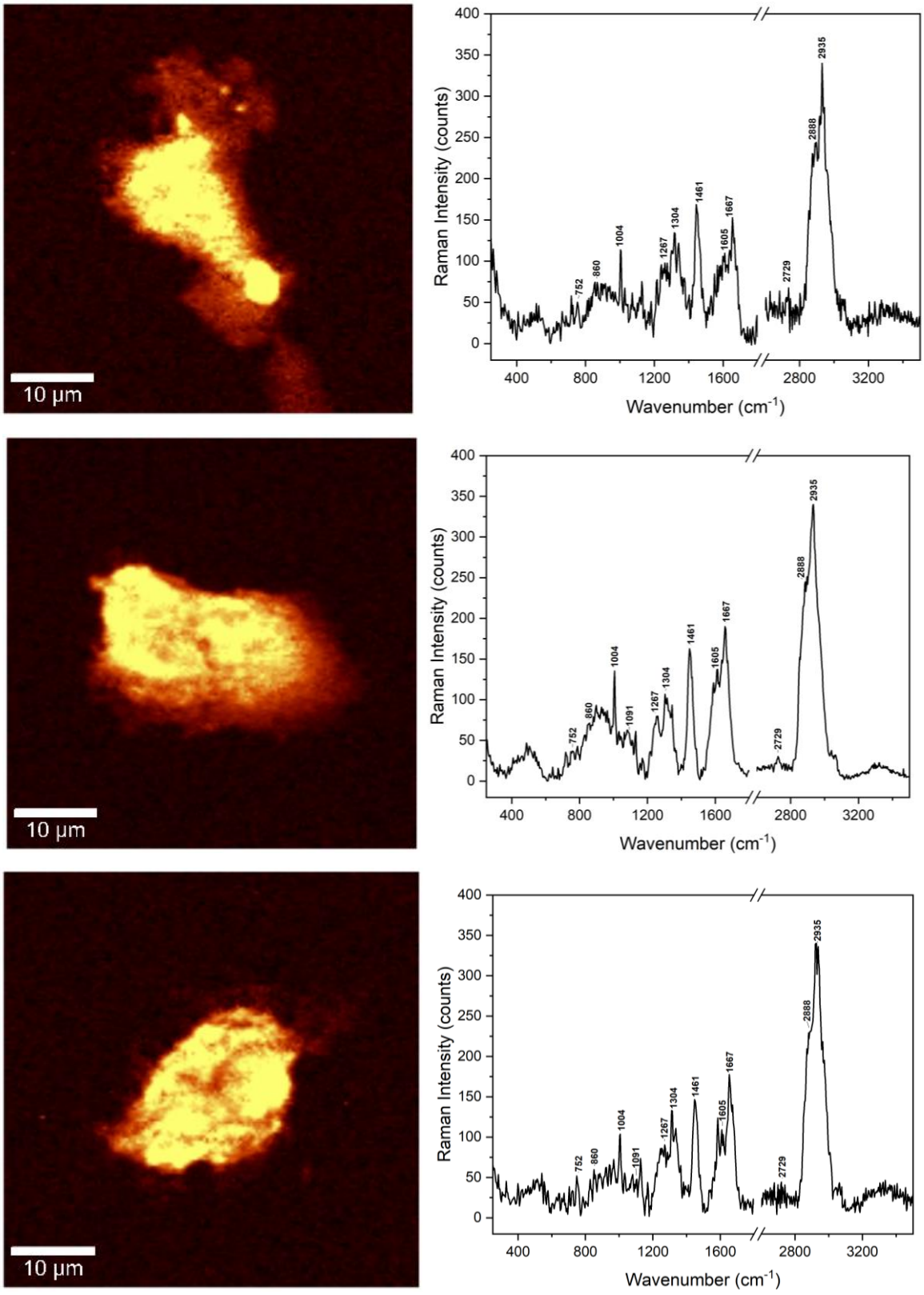

Figure 3.6. Confocal Raman mapping and spectra of 250 µM treated cells.

We can observe noisier signals in Figure 3.6 compared to the individual results shown in Figure 3.4 and Figure 3.2. This is due to the fluorescence caused by the nordihydroguaiaretic acid. Therefore, background subtraction is a crucial process to avoid inconsistency and high error in our results. The average of all five integrated spectra for samples treated with a 250 µM NDGA concentration is presented in Figure 3.7.

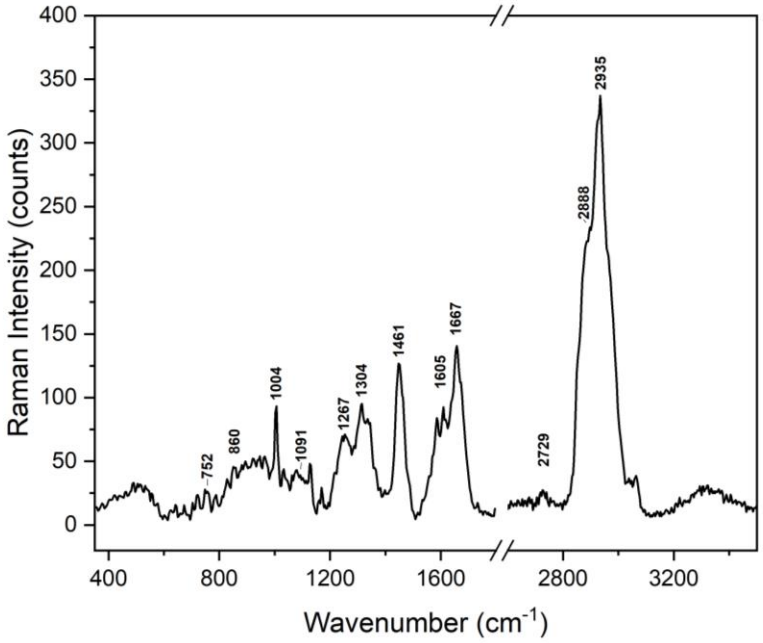

Figure 3.7. Average integrated spectra of 250 µM NDGA-treated cells.

Once again, we observe an increase in the phenylalanine biomarker signal and the protein-to-lipid ratio that will be proved later with the numerical calculations.

3.4 Comparison of Untreated and Treated Cells

The individual results for each sample, give us an overview of what is happening to the cells under the effects of NDGA. However, to have a better understanding, it is important to

compare the average integrated spectra. As mentioned before, we selected five cells for each sample, and we used their individual Raman spectra to obtain an average. Figure 3.8 contains the representative images for the control, the 100 µM, and the 250 µM results.

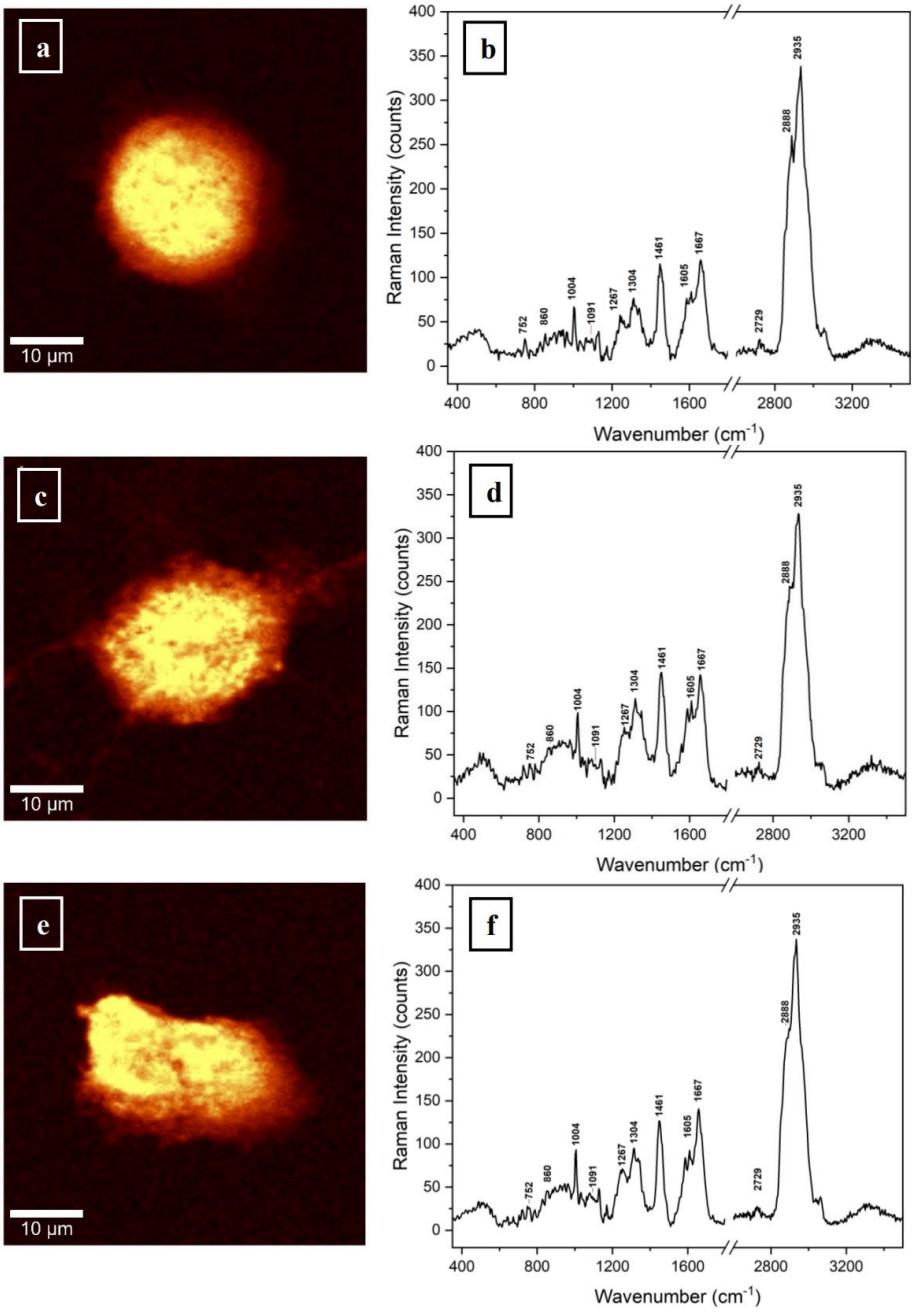

Figure 3.8. Confocal Raman mapping and integrated spectra of untreated (a-b), 100 µM NDGA-treated for 24 h (c-d) and 250 µM NDGA treated for 4 h (e-f) normal astrocyte cells.

To create Figure 3.8, we took representative images of the cell mappings and Figures 3.3, 3.5, and 3.7, which correspond to the Raman integrated spectra. In this way, we can make a better comparison between the results.

As mentioned before, we will focus on the vibrational bands for phenylalanine, lipids, and proteins. By comparing the three spectra in Figure 3.8, we can conclude that NDGA has damaging effects on astrocytes. However, it is smaller compared to the damage that chemotherapy causes. The evidence of damage is seen by the slight increases in the intensities of the peaks at 1004 cm^{-1}, 1461 cm^{-1}, and 1667 cm^{-1}. The 1004 cm^{-1} vibrational line is assigned to phenylalanine, which is an aromatic amino acid. The aromatic amino acids are known to be part of several biological components that serve in the normal functioning of living organisms. Furthermore, researchers have found that the increase of aromatic amino acids can be an indication of cell malignancy, therefore they can be considered as potential biomarkers for cancer and other disorders [31]. The slight increase in the phenylalanine wavenumber is evidence of the cell damage. In addition to this, the Raman line at 1461 cm^{-1}, along with the 2888 cm^{-1} and 2935 cm^{-1} vibrations, is indicative of induced structural modifications affecting lipid and protein content. This observation is also supported by the increase in the intensity of 1667 cm^{-1} peak, which is attributed to amide I [29].

To further understand the differences in the intensities of the 2888 cm^{-1} and 2935 cm^{-1} peaks, we calculated their intensity ratios (I_{2935}/I_{2888}). For the untreated normal astrocytes, we have a ratio of 1.21 ± 0.02. For astrocytes treated with a 100 μM concentration, the ratio is 1.31 ± 0.03. Finally, for the sample with astrocytes treated with a 250 μM NDGA concentration, we obtained a ratio of 1.48 ± 0.04. The increase in this protein-to-lipid ratio suggests a damaging effect of NDGA on the cells, especially at higher concentrations.

So far, we have talked about the Raman spectra. However, an analysis of the mapping can support our spectral results. If we observe Figure 3.8 (a), we have a healthy cell with an intact membrane, as expected. The mapping shown in Figure 3.8 (c), is that of a cell that is starting to get damaged, as we concluded with the integrated spectra, the damage is slight. On the other hand, Figure 3.8 (e), shows an unhealthy cell, the membrane is no longer intact. The damage caused by NDGA at higher concentrations is more significant.

We can conclude that, similarly to the results of our previous research (NDGA effects on GBM), a treatment with repetitive smaller NDGA dosages over a longer period is still recommended. Even though we proved that NDGA has a damaging effect on normal tissue, this damage is less compared to other highly invasive treatments such as chemotherapy. The benefic effects of NDGA on glioblastoma are remarkable. Therefore, we can say with certainty that NDGA could be another potential alternative for non-invasive brain cancer treatment.

Chapter 4: Conclusions

For a long time, cancer has been a target in the research community. Without question, impressive advances have been done. However, the prognosis and patient survival rate remain indicative factors that there are still improvements to be made. Current cancer diagnostic and treatment techniques had been the most valuable player in the health area but is not a secret that most of these methods are highly invasive and, some of them, difficult to perform. In hopes of finding better alternatives, researchers remain focused on this problem. Several studies had found different diagnostic methods that could be the alternative we are looking for. Between these methods, we can find Raman spectroscopic and microscopic techniques.

In recent years, Raman spectroscopy and microscopy have been proven to excel in diagnosing and discriminating between normal and cancerous (or damaged) tissue. As an intraoperative technique, Raman spectroscopy is efficient, with a sensitivity of 93% and a specificity of 91%. However, there are still some limitations that scientists are looking to improve, so the technique can be practical in clinical applications. Scientists agree that to succeed, further in-vivo and in-vitro studies need to be done [13].

The results presented in this project are another proof of Raman's efficiency as a label-free technique. The beauty of confocal Raman microscopy relies on the advantage of measuring samples without prior preparation. The Raman spectra is a fingerprint that gives the needed information to analyze and further know the samples. In our case, it was a magnificent method to discriminate between cancerous and non-cancerous cells and to identify the effects that nordihydroguaiaretic acid (NDGA) has in these two types of cells.

Through this project, we have mentioned that glioblastoma (GBM) is the most devastating brain tumor. Therefore, the motivation to develop this research relies on finding a better alternative to treat this aggressive cancer. Traditional medicine is an extensive area that indigenous people, through their beliefs and experiences, have developed. Natural remedies remain being passed through generations. With the advances in science and technology, several researchers have focused on supporting with scientific facts the benefits of traditional medicine, led by the thought that, with further understanding and control of these natural treatments, a better alternative to treat several diseases can arise. As an example, our research consisted in analyzing the effects of NDGA chemical extract from *Larrea Tridentata* on GBM and astrocytes, through the utilization of confocal Raman microscopy.

Previously, we demonstrated that NDGA has therapeutic effects on GBM. From the two different concentrations (100 μM and 250 μM), we concluded that treatment with a small dosage for a longer period has a better outcome, and thus is recommended, while the higher dosage induces cell and membrane damage. Similar to these concluding remarks, we analyzed astrocyte cells. In this case, we observed that NDGA has damaging effects on the tissue. However, once again, a smaller dosage over longer periods is recommended due to the less damage caused compared to the higher concentration. We were able to have these conclusions, thanks to the observations in the discrepancies and changes of the biological compounds' spectral lines, such as phenylalanine, protein, and lipid ratios that, supported by literature, are some of the main biomarkers in different types of cancer.

The nordihydroguaiaretic acid cytotoxicity remains to be a valid concern. However, we demonstrated that, even though NDGA has a damaging effect on astrocytes, it is less than the damage generated with chemotherapy. Therefore, the findings in this research, are a demonstration

of NDGA as a potential non-invasive brain cancer treatment. In general, further research, in-vivo and in-vitro must be performed to continue understanding the NDGA activity on living organisms. These steps can lead to the development of a new and controlled drug to treat cancer.

Finally, as a continuation of this project and similar to the previous research regarding GBM, a deeper and unbiased analysis can be done by performing principal component analysis (PCA). This statistical technique can be a complement to our experimental analysis and conclusions, since it does not take into account the Raman spectra tentative assignments, on the contrary PCA takes these assignments as variables. Therefore, it is unbiased of previous knowledge [29].

References

[1] Hubbard, J. A., & Binder, D. K. (2016). *Astrocytes and Epilepsy*. Academic Press. pp. 40.

[2] Scemes, E., & Spray, D. C. (2012). *Astrocytes: Wiring the Brain*. Boca Raton: CRC Press. pp. 4.

[3] Blausen.com staff. (2014). *Medical gallery of Blausen Medical 2014*. WikiJournal of Medicine 1 (2). DOI:10.15347/wjm/2014.010. ISSN 2002-4436. License CC by 3.0. https://creativecommons.org/licenses/by/3.0/deed.en

[4] Jäkel, S., & Dimou, L. (2017). *Glial Cells and Their Function in the Adult Brain: A Journey through the History of Their Ablation*. Front. Cell. Neurosci. Vol. 11. pp. 1, 5-8.

[5] Hasel, P., & Liddelow, S.A. (2021). *Astrocytes*. Current Biology. Vol. 31. pp. R326-R327.

[6] Trujillo-Estrada, L., et. al. (2019). *Astrocytes: From the Physiology to the Disease*. Current Alzheimer Research. Vol. 16. pp. 1-3.

[7] Di Benedetto, B. (2019). *Astrocytes: Methods and Protocols*. Methods in Molecular Biology. Vol. 1938. Human Press. pp. 3.

[8] Sofroniew, M.V., & Vinters, H.V. (2010). *Astrocytes: biology and pathology*. Acta Neuropathologica. 119. pp. 8, 11.

[9] Liu, D. (2017). *Tumors and Cancers Central and Peripheral Nervous Systems*. Boca Raton: CRC Press. pp. 1-5, 10-14.

[10] Hirtz, A., et. al. (2020). *Astrocytoma: A Hormone-Sensitive Tumor?* International Journal of Molecular Sciences. Vol. 21. pp. 1.

[11] Baert, R., & Odle, T. G. (2022). *The Gale Encyclopedia of Genetic Disorders*. Gale, a Cangage Company. Vol. 1. 5th ed.

[12] Hayat, M. A. (2012). *Tumors of the Nervous Central System*. Springer. Vol. 8. pp. 13, 14.

[13] Kowalska, A. A., et. al. (2020). *Raman spectroscopy: Discrimination among healthy and cancer cells*. Spectrochimica Acta Part A: Molecular and Biomolecular Spectroscopy. Vol. 231.

[14] Beleites, C., Geiger, K., Kirsch, M. et al. (2011). *Raman spectroscopic grading of astrocytoma tissues: using soft reference information*. *Anal Bioanal Chem*. Vol. 400.

[15] Tanahashi, K., Natsume, A., et. al. (2014). *Assessment of Tumor Cells in a Mouse Model of Diffuse Infiltrative Glioma by Raman Spectroscopy*. BioMed Research International. Vol. 2014.

[16] Banerjee, H. N., & Zhang, L. (2007). *Deciphering the finger Prints of Brain Cancer Astrocytoma in comparison to Astrocytes by using near infrared Raman Spectroscopy*. Molecular and Cellular Biochemistry. Vol. 295

[17] Manda, G., Rojo, A. I., et. al. (2020). *Nordihydroguaiaretic Acid: From Herbal Medicine to Clinical Development for Cancer and Chronic Diseases*. Front. Pharmacol. Vol. 11.

[18] Arteaga, S., Andrade-Cetto, A., & Cardenas, R. (2005). *Larrea tridentata (Creosote Bush), an abundant plant of Mexican and US-American deserts and its metabolite nordihydroguaiaretic acid*. Journal of Ethnopharmacology. Vol 98. pp 231-239.

[19] Smith, E., & Dent, G. (2005). *Modern Raman Spectroscopy - A Practical Approach*. Chichester, West Sussex, United Kingdom: Wiley. pp. 1-4.

[20] Larkin, P. (2011). *Infrared and Raman Spectroscopy: Principles and Spectral Interpretation*. Saint Louis: Elsevier. pp. 1, 2

[21] Hoffmann, G. (2017). *Raman Spectroscopy: Principles and Applications in Chemistry, Physics, Materials Science, and Biology Vol. I*. New York: Momentum Press. pp. 7-11

[22] Ferraro, J. R., Nakamoto, K., & Brown, C. W. (2003). *Introductory Raman Spectroscopy*. Boston: Academic Press. pp. 1, 3.

[23] Vandenabeele, P. (2013). *Practical Raman Spectroscopy: An Introduction*. Chichester, West Sussex, United Kingdom: Wiley. pp. 1-5.

[24] Electromagnetic waves by DECHAMMAKL, distributed under a CC BY-SA 4.0 license. https://creativecommons.org/licenses/by-sa/4.0/deed.en

[25] Toporski J., Dieing T., & Hollricher, O. (2018) *Confocal Raman Microscopy*. Berlin, Heidelberg: Springer. pp. 25-26, 69-72.

[26] Zhu, X., Xu, T., Lin, Q., & Duan, Y. (2014). *Technical Development of Raman Spectroscopy: From Instrumental to Advanced Combined Technologies*. Applied Spectroscopy Reviews. 49. 64-82. 10.1080/05704928.2013.798801. pp. 65, 66, 72.

[27] WITec focus innovations. (2008) *System Description*. Germany: WITec Wissenschaftliche Instrumente und Technologie GmbH. pp. 3-20.

[28] WITec focus innovations. (2008). Germany: WITec Wissenschaftliche Instrumente und Technologie GmbH. pp. 5-6.

[29] Manciu, F. S., et. al. (2022). *Assessing Nordihydroguaiaretic Acid Therapeutic Effect for Glioblastoma Multiforme*. Sensors (Basel).

[30] Iturrioz-Rodriguez, N., et. al. (2022). *Discrimination of glioma patient-derived cells from healthy astrocytes by exploiting Raman spectroscopy*. Spectrochimica Acta Part A: Molecular and Biomolecular Spectroscopy. Vol. 269. pp. 5.

[31] Contorno, S., Darienzo, R.E., & Tannenbaum, R. (2021). *Evaluation of aromatic amino acids as potential biomarkers in breast cancer by Raman spectroscopy analysis*. Scientific Reports. Vol. 11.

Vita

Lizbeth Vanessa Martinez Lopez was born in Mexico in 1997. In 2019, she earned her bachelor's degree in physics at the Universidad of Sonora. During her undergraduate studies, she was part of a tutoring program in the Department of Physics, where she helped other students in different math and physics subjects. She also participated in a summer research program of the *Programa Delfín*, where she worked under the supervision of Dr. Ricardo Lopez Esparza on a Neuronal Biophysics project. She started her master's degree in physics at the University of Texas at El Paso in the spring of 2021. During her master's studies, she worked as a teaching assistant. She joined the Optical Spectroscopy and Microscopy laboratory, where she worked under the supervision of Dr. Felicia Manciu. Here, she co-authored "*Assessing Nordihydroguaiaretic Acid Therapeutic Effect for Glioblastoma Multiforme"* published in Sensors (Basel) in March 2022.

Contact Information: vanessa_martinez_97@hotmail.com